Applied Numerical Mathematics 199 (2024) 59–72

Contents lists available at ScienceDirect

Applied Numerical Mathematics

journal homepage: www.elsevier.com/locate/apnum

Particle trajectories in a weakly nonlinear long-wave model on a shear flow

Olufemi Elijah Ige, Henrik Kalisch *

Department of Mathematics, University of Bergen, Postbox 7800, 5020 Bergen, Norway

ARTICLE INFO

Article history:
Received 31 July 2022
Received in revised form 12 December 2022
Accepted 19 January 2023
Available online 24 January 2023

Keywords:
Surface waves
Particle trajectories
Shear flow
Vorticity
Solitary waves
Cnoidal waves
BBM equation

ABSTRACT

This work centers on the numerical examination of particle trajectories associated with the propagation of long water waves of small but finite amplitude on a background shear flow over a flat bottom. Taking into consideration the assumption that the nonlinear and dispersive effects are small and of the same magnitude, the Boussinesq-type equations for two-dimensional water waves on a background flow with constant vorticity are derived. Restricting attention to waves propagating in a single direction, we find a new version of the Benjamin-Bona-Mahony (BBM) equation which takes into account the effect of vorticity. In order to investigate the particle trajectories of the flow, an approximate velocity field associated with the derivation of the BBM equation over a shear flow is obtained. Several cases of particle paths under surface waves profiles such as solitary waves and periodic traveling waves are examined.

1. Introduction

Boussinesq-type equations are widely used for the simulation of ocean waves in the nearshore zone, where both nonlinear and dispersive effects influence the wave evolution. While these simplified model equations are most often derived in the context of irrotational flow, in coastal waters, the presence of vorticity may also be an important factor. Indeed, a variety of currents exists in the coastal zone, such as for example tidal currents and currents due to river discharge (see [26] for example). In this situation, using the assumption that the flows are irrotational when gravity waves travel on the surface of shear flows is no longer valid [4]. The inclusion of the vorticity to the shallow-water theory was first considered by Burns [7], who modified the shallow-water theory by incorporating the effects of the vorticity and studied the range of wave speeds for general velocity profiles. Following the publication of [37], constant background shear has been used in many works (see for example, [1,11,17,23,38,40,41] and the references therein). A linear shear flow avoids many of the mathematical complications of more general current profiles and may be seen as a first approximation to more general shear currents, especially in the case of long wavelength.

Recently, more general shear profiles have been used for the description of flow properties associated with surface waves (see [9,21,31] for example) in steady form. Other examples of surface waves interacting with vorticity include the case of compactly supported vorticity, such as vortex patches [35] and point vortices [16,18]. One recent work addresses the problem of vorticity creation by the waves itself in the transient case [8], though the resulting mathematical model is rather complex.

* Corresponding author.
E-mail addresses: olufemi.ige@uib.no (O.E. Ige), henrik.kalisch@uib.no (H. Kalisch).

https://doi.org/10.1016/j.apnum.2023.01.016
0168-9274/

In the present work, the goal is to use a simple model equation in order to describe particle trajectories associated with surface wave patterns in the presence of constant vorticity. A series of derivations is carried out, resulting in a BBM-type equation that is valid in the presence of background constant vorticity. The BBM model will be examined in the non-dimensional form

$$\eta_t + c_+\eta_x + \frac{c_+(3+\Gamma^2)}{(1+c_+^2)}\eta\eta_x - \frac{c_+ + \Gamma}{3c_+(1+c_+^2)}\eta_{xxt} = 0,$$

where $\eta(x,t)$ is the surface profile, Γ is the prescribed vorticity, and the constants c_+ and c_- are given by $c_+ = \frac{-\Gamma}{2} + \sqrt{\frac{\Gamma^2}{4}+1}$ and $c_- = \frac{-\Gamma}{2} - \sqrt{\frac{\Gamma^2}{4}+1}$. Except for the coefficients, this equation is similar to the standard BBM equation and can be reduced to a first-order equation for both solitary and periodic (cnoidal) traveling waves in terms of surface elevation. Furthermore, as will be shown presently, a rigorous review of the derivation of the BBM equation as a surface water-wave model in the presence of a background shear flow reveals that the reconstruction of an approximate fluid velocity field below the free surface is possible. This process yields expressions for the horizontal and vertical velocity components in terms of the principal unknown variable η, which represents the deflection of the free surface from the equilibrium position.

To the first order in the perturbation parameter, it is observed that the horizontal velocity is not connected to its measuring depth, and we have $u = -c_-\eta$. However, considering the fact that the BBM equation is accurate to the second order, this term is revised to an expression that holds to the second-order as given below

$$u = -c_-\eta + \frac{c_- + \Gamma}{2(1+c_+^2)}\eta^2 + \left(\frac{c_+ + \Gamma}{3(1+c_+^2)} - \frac{c_-}{6}\right)\eta_{xx}. \tag{1}$$

In (1), the horizontal velocity at the flat bottom is denoted by u. It is also possible to obtain an equation for this horizontal velocity at an arbitrary depth in the fluid column. This theory will be presented in the next section. After establishing the velocity field connected to the surface wave, a great number of the dynamic features of the flow can be exploited, especially the construction of the approximate representations of the trajectories mapped out by the particles of the fluid beneath the surface.

The investigation of particle paths underneath a surface wave can be traced back to the late nineteenth century [30]. In linear wave theory, a standard first-order approximation suggests that all particle paths are closed [19,27,33]. However, Stokes [34] showed that particle trajectories are not closed for periodic waves (see also [10,15]). Indeed, the movement of a periodic surface wave is associated with particle trajectories that are not closed and lead to net mass transport in the direction of the wave. This result is known today as the Stokes drift. Stokes drift in channels of finite depth was reviewed by Ursell [39]. Constantin [12] gave firm mathematical proof that the particle paths are not closed. Other effects, such as infragravity wave motion and inertia, may also affect the particle motion [2,6]. We finally mention the work of Munk who considered particle motion under waves in the surf zone and applied a backward current in order to describe nearly closed particle paths which were observed under some conditions [29].

The first work which made use of Lagrangian coordinates for the examination of periodic surface gravity waves with finite vorticity was Gerstner [20]. In the Gerstner wave, particles travel in circles, and the surface curve is of trochoidal form. The mathematical approach used in [22] shows that Gerstner's flow is dynamically possible: the particles never collide despite moving in a circle and occupy the whole region beneath the surface wave. Later, Constantin and Strauss [14] showed that a closed particle path in the presence of current is possible. There have also been numerical studies of several orbit patterns. Indeed, Nachbin and Ribeiro-Junior [30] investigated a case of a closed orbit when a stokes wave propagates in the presence of an adverse current. Particle paths in shear flow have been studied in various situations using the full Euler equations in a steady formulation [9,21,31]. More recently, physical phenomena such as wave breaking, and undular bores were considered in this context [25,32].

The present study focuses on providing a clear qualitative view of the particle paths throughout the fluid domain of the nonlinear water waves on the shear flows. The article is organized as follows: a thorough review of the derivation of the Boussinesq system that features shear flow is presented in Section 2. Afterward, we sketch the derivation of the BBM equation and its corresponding approximate velocity field in terms of the free surface η and constant vorticity Γ. In Section 3, we study the surface solitary wave. Here, the velocity field expressions derived in Section 2 in connection with the exact solutions of the BBM equation are used to examine the particle trajectories numerically by considering different values of vorticity. Similarly, Section 4 is dedicated to the numerical investigation of the particle trajectories in connection to the propagation of the periodic wave. Lastly, Section 5 is devoted to the conclusion.

2. Formulation of the mathematical problem

The water-wave problem concerning waves at the surface of an inviscid, incompressible Newtonian fluid is given by the Euler equations with no-penetration conditions at the bed and kinematic and dynamic boundary conditions at the free surface. The sea floor is assumed to be flat. We denote the spatial coordinates by (x,z) where the x-axis coincides with the

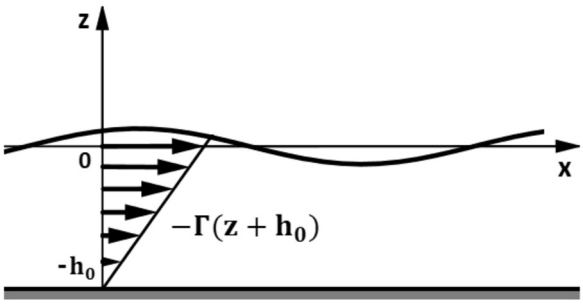

Fig. 1. Wave propagation over a background shear flow. In this figure, the vorticity Γ is negative.

undisturbed free surface, and assume long-crested waves which are uniform in the transverse direction. The gravitational acceleration in the negative z-direction is denoted by g, the undisturbed depth is h_0, and $\eta(x,t)$ denotes the departure of the free surface from the rest position. The decisive feature in the present work is the existence of a uniform shear flow with a free surface as shown in Fig. 1. In this case, the vorticity is given by a predescribed constant Γ, and the background distribution of the original velocity component before the arrival of the waves is given by

$$\left.\begin{array}{rcl} U &=& U_0 - (z+h_0)\Gamma, \\ V &=& 0. \end{array}\right\} \tag{2}$$

For $\Gamma > 0$, we have a shear flow in the direction opposite to the wave propagation. For $\Gamma < 0$, the background flow is in the favorable direction, that is, in the direction of wave propagation. Without loss of generality, we may assume $U_0 = 0$. Assuming a is a typical amplitude, and l is a typical wavelength of the waves to be described, the parameter $\alpha = a/h_0$ represents the amplitude to depth ratio, and the parameter $\beta = h_0^2/l^2$ represents the water depth to wavelength ratio.

In the case of a linear shear flow such as delineated in (2), the vorticity is constant. For later reference, we define the unit vectors in the x, y and z directions as $\mathbf{e}_x$, $\mathbf{e}_y$ and $\mathbf{e}_z$, respectively. The vorticity is then given by $\omega = (U_z - V_x)\mathbf{e}_y = -\Gamma\mathbf{e}_y$. In general, one may use Kelvin's circulation theorem together with Stokes theorem and the incompressibility condition to understand that constant vorticity is conserved in inviscid, incompressible flow. In consequence, the flow can be split into a shear flow with uniform vorticity and a pure potential flow. For a uniform shear flow, the perturbation velocity is given in terms of the potential $\phi(x,z,t)$, with $u = \phi_x$ and $v = \phi_z$. The complete velocity field is given by

$$\left.\begin{array}{c} U = \phi_x - (z+h_0)\Gamma, \\ V = \phi_z. \end{array}\right\}$$

Indeed if we define a three-dimensional velocity field $\mathbf{U} = (U, 0, V)$ for notational convenience, the vorticity is $\omega = \mathrm{curl}(\mathbf{U})$, and it can be checked that the above definition satisfies the vorticity equation

$$\omega_t + (\mathbf{U}\cdot\nabla)\omega = \omega\cdot\nabla\mathbf{U}. \tag{3}$$

Using the incompressibility condition $\nabla\cdot\mathbf{U} = 0$ also shows that the velocity potential satisfies Laplace's equation. We can then rewrite the Euler equations

$$\mathbf{U}_t + \frac{1}{2}\nabla|\mathbf{U}|^2 - \mathbf{U}\times\omega + ge_z = 0$$

with the help of the velocity potential ϕ to obtain

$$\nabla\left\{\phi_t + \frac{1}{2}|\mathbf{U}|^2 + gz\right\} = \mathbf{U}\times\omega.$$

As the left-hand side is obviously a gradient, the term $\mathbf{U}\times\omega$ must also be the gradient of a function. Following [42] it becomes plain that $\mathbf{U}\times\omega = \nabla G$, where the function G is given by

$$G = -\Gamma\int_{-h_0}^{z}\phi_x\,dz + \frac{\Gamma^2}{2}(z+h_0)^2.$$

The complete problem is written as follows:

$$\Delta\phi = 0 \qquad \text{in } -h_0 < z < \eta(x,t), \tag{4}$$

$$\phi_z = 0 \qquad \text{on } z = -h_0, \tag{5}$$

$$\left.\begin{array}{c} \eta_t + U\eta_x - V = 0, \\ \phi_t + \frac{1}{2}|\mathbf{U}|^2 - G + g\eta = 0, \end{array}\right\} \quad \text{on } z = \eta(x,t). \tag{6}$$

The next goal is to derive a Boussinesq system approximating the wave motion described by (4)-(6). To this end, we follow the development explained in [42]. For starters, the variables are non-dimensionalized using the following scaling:

$$\tilde{x} = \frac{x}{l}, \quad \tilde{z} = \frac{z}{h_0}, \quad \tilde{t} = \frac{\sqrt{gh_0}t}{l}, \quad \tilde{\Gamma} = \frac{\Gamma h_0}{\sqrt{gh_0}}, \quad \tilde{\eta} = \frac{\eta}{a}, \quad \tilde{\phi} = \frac{h_0}{al\sqrt{gh_0}}\phi.$$

Then we get the equation

$$\beta\tilde{\phi}_{\tilde{x}\tilde{x}} + \tilde{\phi}_{\tilde{z}\tilde{z}} = 0 \quad -1 < \tilde{z} < \alpha\tilde{\eta}, \tag{7}$$

and at the bottom $\tilde{z} = -1$, we have the following boundary condition

$$\tilde{\phi}_{\tilde{z}} = 0. \tag{8}$$

At the free surface $\tilde{z} = \alpha\tilde{\eta}$, the non-dimensional kinematic condition is

$$\beta\left\{\tilde{\eta}_{\tilde{t}} + \left[-(1+\alpha\tilde{\eta})\tilde{\Gamma} + \alpha\tilde{\phi}_{\tilde{x}}\right]\tilde{\eta}_{\tilde{x}}\right\} = \tilde{\phi}_{\tilde{z}}. \tag{9}$$

The non-dimensional dynamic condition may be expressed as

$$\beta(\tilde{\phi}_{\tilde{t}} + \tilde{\eta}) + \frac{\alpha\beta}{2}\left[\tilde{\phi}_{\tilde{x}} - \frac{\tilde{\Gamma}}{\alpha}(1+\alpha\tilde{\eta})\right]^2 + \frac{\alpha}{2}\left[\tilde{\phi}_{\tilde{z}}\right]^2 - \frac{\beta}{ag}G = 0. \tag{10}$$

The non-dimensional potential $\tilde{\phi}$ is expressed in powers of $(1+\tilde{z})$ as

$$\tilde{\phi} = \sum_{n=0}^{\infty}(1+\tilde{z})^n\phi_n. \tag{11}$$

Using Eq. (7), Eq. (11) and Eq. (8), we have

$$\tilde{\phi} = \phi_0 - \frac{\beta}{2}(1+\tilde{z})^2\phi_{0\tilde{x}\tilde{x}} + \frac{\beta^2}{24}(1+\tilde{z})^4\phi_{0\tilde{x}\tilde{x}\tilde{x}\tilde{x}} + \mathcal{O}(\beta^3). \tag{12}$$

To find a closed system of two evolution equations, we substitute the asymptotic expression for $\tilde{\phi}$ in the boundary conditions Eq. (9) and Eq. (10) and collect all terms of zeroth and first-order in α and β. Then we differentiate the dynamic bottom boundary with respect to $\tilde{x}$ and expressed the boundary conditions in terms of the non-dimensional horizontal velocity at the bottom $\phi_{0\tilde{x}} = \tilde{w}$. This procedure yields the system of equations

$$\begin{aligned}\tilde{\eta}_{\tilde{t}} + \tilde{w}_{\tilde{x}} - \tilde{\Gamma}\tilde{\eta}_{\tilde{x}} - \alpha\tilde{\Gamma}\tilde{\eta}\tilde{\eta}_{\tilde{x}} + \alpha(\tilde{\eta}\tilde{w})_{\tilde{x}} - \frac{\beta}{6}\tilde{w}_{\tilde{x}\tilde{x}\tilde{x}} &= \mathcal{O}(\alpha\beta, \beta^2),\\ \tilde{w}_{\tilde{t}} + \tilde{\eta}_{\tilde{x}} + \alpha\tilde{w}\tilde{w}_{\tilde{x}} - \frac{\beta}{2}\tilde{w}_{\tilde{x}\tilde{x}\tilde{t}} + \frac{\beta}{3}\tilde{\Gamma}\tilde{w}_{\tilde{x}\tilde{x}\tilde{x}} &= \mathcal{O}(\alpha\beta, \beta^2).\end{aligned} \tag{13}$$

Next, a family of Boussinesq systems is derived using the standard technique of describing the horizontal velocity component at different heights in the fluid column. If we let $\tilde{w}^\theta$ be the non-dimensional velocity at a non-dimensional height $\tilde{z}_\theta = -1 + \theta(\alpha\tilde{\eta} + 1)$, with $0 \le \theta \le 1$, then Taylor's formula shows that

$$\tilde{w}^\theta = \tilde{w} - \frac{\beta}{2}(1+\tilde{z}_\theta)^2\tilde{w}_{\tilde{x}\tilde{x}} + \mathcal{O}(\beta^2) = \tilde{w} - \frac{\beta}{2}\theta^2\tilde{w}_{\tilde{x}\tilde{x}} + \mathcal{O}(\alpha\beta, \beta^2).$$

By applying the standard techniques of inversion, it is not difficult to derive the following expression as an asymptotic formula for $\tilde{w}$ in terms of $\tilde{w}^\theta$:

$$\tilde{w} = \tilde{w}^\theta + \frac{\beta}{2}\theta^2\tilde{w}^\theta_{\tilde{x}\tilde{x}} + \mathcal{O}(\alpha\beta, \beta^2). \tag{14}$$

Substituting this representation into the system (13), this yields

$$\begin{aligned}\tilde{\eta}_{\tilde{t}} + \tilde{w}^\theta_{\tilde{x}} - \tilde{\Gamma}\tilde{\eta}_{\tilde{x}} - \alpha\tilde{\Gamma}\tilde{\eta}\tilde{\eta}_{\tilde{x}} + \alpha(\tilde{\eta}\tilde{w}^\theta)_{\tilde{x}} + \frac{\beta}{2}(\theta^2 - \tfrac{1}{3})\tilde{w}^\theta_{\tilde{x}\tilde{x}\tilde{x}} &= \mathcal{O}(\alpha\beta, \beta^2),\\ \tilde{w}^\theta_{\tilde{t}} + \tilde{\eta}_{\tilde{x}} + \alpha\tilde{w}^\theta\tilde{w}^\theta_{\tilde{x}} + \frac{\beta}{2}(\theta^2 - 1)\tilde{w}^\theta_{\tilde{x}\tilde{x}\tilde{t}} + \frac{\beta}{3}\tilde{\Gamma}\tilde{w}^\theta_{\tilde{x}\tilde{x}\tilde{x}} &= \mathcal{O}(\alpha\beta, \beta^2).\end{aligned} \tag{15}$$

For any real λ and μ, the above system is a special case of the more general system

$$\tilde{\eta}_{\tilde{t}} + \tilde{w}^{\theta}_{\tilde{x}} - (1+\alpha\tilde{\eta})\tilde{\Gamma}\tilde{\eta}_{\tilde{x}} + \alpha(\tilde{\eta}\tilde{w}^{\theta})_{\tilde{x}} + \frac{\beta}{2}(\theta^2 - \tfrac{1}{3})\lambda\tilde{w}^{\theta}_{\tilde{x}\tilde{x}\tilde{x}} - \tfrac{\beta}{2}(\theta^2 - \tfrac{1}{3})(1-\lambda)\tilde{\eta}_{\tilde{x}\tilde{x}\tilde{t}} + \frac{\beta}{2}(\theta^2 - \tfrac{1}{3})(1-\lambda)\tilde{\Gamma}\tilde{\eta}_{\tilde{x}\tilde{x}\tilde{x}} = \mathcal{O}(\alpha\beta, \beta^2),$$

$$\tilde{w}^{\theta}_{\tilde{t}} + \tilde{\eta}_{\tilde{x}} + \alpha\tilde{w}^{\theta}\tilde{w}^{\theta}_{\tilde{x}} + \frac{\beta}{2}(1-\theta^2)\mu\tilde{\eta}_{\tilde{x}\tilde{x}\tilde{x}} - \frac{\beta}{2}(1-\theta^2)(1-\mu)\tilde{w}^{\theta}_{\tilde{x}\tilde{x}\tilde{t}} + \frac{\beta}{3}\tilde{\Gamma}\tilde{w}^{\theta}_{\tilde{x}\tilde{x}\tilde{x}} = \mathcal{O}(\alpha\beta, \beta^2).$$

The concentration is now on the unidirectional waves. In the lowest order, the Boussinesq equation is the linear system

$$\tilde{\eta}_{\tilde{t}} + \tilde{w}^{\theta}_{\tilde{x}} - \tilde{\Gamma}\tilde{\eta}_{\tilde{x}} = 0, \quad \tilde{w}^{\theta}_{\tilde{t}} + \tilde{\eta}_{\tilde{x}} = 0. \tag{16}$$

The system can be diagonalized by introducing characteristic coordinates. Introduce new variables r and s defined by $(r,s) = P^{-1}(\tilde{\eta}, \tilde{w}^{\theta})$ where

$$P^{-1} = \frac{1}{1+(\tilde{c}_+)^2}\begin{pmatrix} \tilde{c}_+ & 1 \\ -1 & \tilde{c}_+ \end{pmatrix},$$

with $\tilde{c}_+ = \frac{-\tilde{\Gamma}}{2} + \sqrt{\frac{\tilde{\Gamma}^2}{4}+1}$. A simple calculation shows that

$$\begin{pmatrix} r_t \\ s_t \end{pmatrix} + \begin{pmatrix} \tilde{c}_+ & 0 \\ 0 & \tilde{c}_- \end{pmatrix}\begin{pmatrix} r_x \\ s_x \end{pmatrix} = 0 \tag{17}$$

where $\tilde{c}_- = \frac{-\tilde{\Gamma}}{2} - \sqrt{\frac{\tilde{\Gamma}^2}{4}+1}$ is the conjugate of $\tilde{c}_+$. The solutions of system (17) are

$$r = r_0(x - \tilde{c}_+ t) \text{ and } s = s_0(x - \tilde{c}_- t).$$

The solution to Eq. (16) is, therefore,

$$\tilde{w}^{\theta}(x,t) = \frac{1}{1+\tilde{c}_+^2}\Big[\tilde{c}_+\tilde{\eta}_0(x-\tilde{c}_+t) + \tilde{w}^{\theta}_0(x-\tilde{c}_+t) - \tilde{c}_+\tilde{\eta}_0(x-\tilde{c}_-t) + \tilde{c}_+^2\tilde{w}^{\theta}_0(x-\tilde{c}_-t)\Big],$$

$$\tilde{\eta}(x,t) = \frac{1}{1+\tilde{c}_+^2}\Big[\tilde{c}_+^2\tilde{\eta}_0(x-\tilde{c}_+t) + \tilde{c}_+\tilde{w}^{\theta}_0(x-\tilde{c}_+t) + \tilde{\eta}_0(x-\tilde{c}_-t) - \tilde{c}_+\tilde{w}^{\theta}_0(x-\tilde{c}_-t)\Big].$$

The unidirectional KdV equation is derived from the system (15) by specializing to waves moving to the right with speed $\tilde{c}_+$.

$$\tilde{w}^{\theta} = -\tilde{c}_-\tilde{\eta} + \alpha A + \beta B + \mathcal{O}(\alpha\beta, \beta^2),$$

where A and B are functions of $\tilde{\eta}$ and its $\tilde{x}$ derivatives. Then the system (15) becomes

$$\tilde{\eta}_{\tilde{t}} + \tilde{c}_+\tilde{\eta}_{\tilde{x}} + \alpha(-2\tilde{c}_-\tilde{\eta}\tilde{\eta}_{\tilde{x}} - \tilde{\Gamma}\tilde{\eta}\tilde{\eta}_{\tilde{x}} + A_{\tilde{x}}) + \beta(B_{\tilde{x}} - \tfrac{1}{2}\tilde{c}_-(\theta^2 - \tfrac{1}{3})\tilde{\eta}_{\tilde{x}\tilde{x}\tilde{x}}) = \mathcal{O}(\alpha\beta, \beta^2),$$

$$\tilde{\eta}_{\tilde{t}} + \tilde{c}_+\tilde{\eta}_{\tilde{x}} + \alpha(\tilde{c}_+A_{\tilde{t}} - \tilde{c}_-\tilde{\eta}\tilde{\eta}_{\tilde{x}}) + \beta(\tilde{c}_+B_{\tilde{t}} + \tfrac{1}{2}(\theta^2-1)\tilde{\eta}_{\tilde{x}\tilde{x}\tilde{t}} + \tfrac{\tilde{\Gamma}}{3}\tilde{\eta}_{\tilde{x}\tilde{x}\tilde{x}}) = \mathcal{O}(\alpha\beta, \beta^2).$$

Since $\tilde{\eta}_{\tilde{t}} = -\tilde{c}_+\tilde{\eta}_{\tilde{x}}$, all derivatives in the first order terms may be replaced by $-\tilde{c}_+$ times the x derivatives. Then the two equations are consistent if

$$A = \frac{\tilde{c}_- + \tilde{\Gamma}}{2(1+\tilde{c}_+^2)}\tilde{\eta}^2 \text{ and } B = \left(\frac{\tilde{c}_+ + \tilde{\Gamma}}{3(1+\tilde{c}_+^2)} - \frac{\tilde{c}_-}{6} + \frac{\tilde{c}_-}{2}\theta^2\right)\tilde{\eta}_{\tilde{x}\tilde{x}}.$$

Hence, we have

$$\begin{aligned} \tilde{w}^{\theta} &= -\tilde{c}_-\tilde{\eta} + \alpha\frac{\tilde{c}_- + \tilde{\Gamma}}{2(1+\tilde{c}_+^2)}\tilde{\eta}^2 + \beta\left(\frac{\tilde{c}_+ + \tilde{\Gamma}}{3(1+\tilde{c}_+^2)} - \frac{\tilde{c}_-}{6} + \frac{\tilde{c}_-}{2}\theta^2\right)\tilde{\eta}_{\tilde{x}\tilde{x}} + \mathcal{O}(\alpha\beta, \beta^2), \\ \tilde{\eta}_{\tilde{t}} &+ \tilde{c}_+\tilde{\eta}_{\tilde{x}} + \alpha\frac{\tilde{c}_+(3+\tilde{\Gamma}^2)}{(1+\tilde{c}_+^2)}\tilde{\eta}\tilde{\eta}_{\tilde{x}} + \beta\frac{\tilde{c}_+ + \tilde{\Gamma}}{3(1+\tilde{c}_+^2)}\tilde{\eta}_{\tilde{x}\tilde{x}\tilde{x}} = \mathcal{O}(\alpha\beta, \beta^2). \end{aligned} \tag{18}$$

From Eq. (14), the non-dimensional horizontal velocity at the bottom is

$$\tilde{w} = -\tilde{c}_-\tilde{\eta} + \alpha\frac{\tilde{c}_- + \tilde{\Gamma}}{2(1+\tilde{c}_+^2)}\tilde{\eta}^2 + \beta\frac{\tilde{c}_+ + \tilde{\Gamma}}{3(1+\tilde{c}_+^2)}\tilde{\eta}_{\tilde{x}\tilde{x}} - \tilde{c}_-\frac{\beta}{6}\tilde{\eta}_{\tilde{x}\tilde{x}} + \mathcal{O}(\alpha\beta, \beta^2). \tag{19}$$

From Eq. (12), the non-dimensional horizontal velocity and the non-dimensional vertical velocity at the bottom become

$$\begin{aligned}\tilde{u} &= \tilde{w} - \frac{\beta}{2}(1+\tilde{z})^2\tilde{w}_{\tilde{x}\tilde{x}} + \mathcal{O}(\beta^2),\\ \tilde{v} &= -\beta(1+\tilde{z})\tilde{w}_{\tilde{x}\tilde{x}} + \mathcal{O}(\beta^2).\end{aligned} \tag{20}$$

From Eq. (14) and Eq. (20), the non-dimensional horizontal velocity and the non-dimensional vertical velocity at a non-dimensional height $\tilde{z}_\theta = -1 + \theta(\alpha\tilde{\eta}+1)$ become

$$\begin{aligned}\tilde{u} &= \tilde{w}^\theta + \frac{\beta}{2}\left(\theta^2 - (1+\tilde{z}_\theta)^2\right)\tilde{w}^\theta_{\tilde{x}\tilde{x}} + \mathcal{O}(\beta^2),\\ \tilde{v} &= -\beta(1+\tilde{z}_\theta)\tilde{w}^\theta_{\tilde{x}} + \mathcal{O}(\beta^2).\end{aligned}$$

From Eq. (19) and Eq. (20), we have

$$\begin{aligned}\tilde{u} &= -\tilde{c}_-\tilde{\eta} + \alpha\frac{\tilde{c}_- + \tilde{\Gamma}}{2(1+\tilde{c}_+^2)}\tilde{\eta}^2 + \beta\frac{\tilde{c}_+ + \tilde{\Gamma}}{3(1+\tilde{c}_+^2)}\tilde{\eta}_{\tilde{x}\tilde{x}} - \tilde{c}_-\frac{\beta}{6}\tilde{\eta}_{\tilde{x}\tilde{x}} + \tilde{c}_-\frac{\beta}{2}(1+\tilde{z})^2\tilde{\eta}_{\tilde{x}\tilde{x}} + \mathcal{O}(\alpha\beta,\beta^2),\\ \tilde{v} &= \beta\tilde{c}_-\tilde{\eta}_{\tilde{x}}(1+\tilde{z}) + \mathcal{O}(\alpha\beta,\beta^2).\end{aligned}$$

After neglecting the second-order term, the dimensional form of the velocities is given by

$$\begin{aligned}u &= \sqrt{\frac{g}{h_0}}\left\{-\tilde{c}_-\eta + \frac{\tilde{c}_- + \tilde{\Gamma}}{2(1+\tilde{c}_+^2)}\frac{\eta^2}{h_0} + \frac{\tilde{c}_+ + \tilde{\Gamma}}{3(1+\tilde{c}_+^2)}h_0^2\eta_{xx} - \frac{\tilde{c}_-}{6}{h_0}^2\eta_{xx} + \frac{\tilde{c}_-}{2}h_0^2(1+\frac{z}{h_0})^2\eta_{xx}\right\},\\ v &= \sqrt{gh_0}\,\tilde{c}_-\,\eta_x\left(1+\frac{z}{h_0}\right).\end{aligned} \tag{21}$$

In the following, it will be convenient to define non-dimensional variables adapted to the problem at hand. In particular, a new non-dimensionalization adapted to the numerical study is defined by

$$x \to h_0 x,\ z \to h_0 z,\ \eta \to h_0\eta,\ t \to \frac{h_0}{\sqrt{gh_0}}t,\ u \to \sqrt{gh_0}u,\ w \to \sqrt{gh_0}w,\ \text{ and } \Gamma \to \frac{\Gamma\sqrt{gh_0}}{h_0}.$$

Then Eq. (21) can be rewritten in terms of new variables as

$$\begin{aligned}u &= -c_-\eta + \frac{c_- + \Gamma}{2(1+c_+^2)}\eta^2 + \frac{c_+ + \Gamma}{3(1+c_+^2)}\eta_{xx} - \frac{c_-}{6}\eta_{xx} + \frac{c_-}{2}(1+z)^2\eta_{xx},\\ v &= c_-\eta_x\,(1+z).\end{aligned}$$

The coefficients are given as $c_+ = \frac{-\Gamma}{2} + \sqrt{\frac{\Gamma^2}{4}+1}$ and $c_- = \frac{-\Gamma}{2} - \sqrt{\frac{\Gamma^2}{4}+1}$. The Eq. (18) can be rewritten in terms of new variables as

$$\eta_t + c_+\eta_x + \frac{c_+(3+\Gamma^2)}{(1+c_+^2)}\eta\eta_x + \frac{c_+ + \Gamma}{3(1+c_+^2)}\eta_{xxx} = 0. \tag{22}$$

This equation was also found in [32,36]. By neglecting the nonlinear term as well as the higher-order term, the resulting equation is given as $\eta_t + c_+\eta_x = 0$. Upon differentiating both sides, we have $\eta_{xxx} = -\frac{1}{c_+}\eta_{xxt}$. Using this in equation (22) yields the BBM equation with vorticity

$$\eta_t + c_+\eta_x + \frac{c_+(3+\Gamma^2)}{(1+c_+^2)}\eta\eta_x - \frac{c_+ + \Gamma}{3c_+(1+c_+^2)}\eta_{xxt} = 0. \tag{23}$$

This equation is the main model used in this article. The expressions for the horizontal and vertical velocities of a fluid particle at a height $z = -1 + \theta(\eta+1)$ are given in new variables as

$$\begin{aligned}u(x,z,t) &= w^\theta(x,t) + \frac{1}{2}\left(\theta^2 - (1+z)^2\right)w^\theta_{xx},\\ v(x,z,t) &= -(1+z)w^\theta_x,\end{aligned} \tag{24}$$

where

$$w^\theta = -c_-\eta + \frac{c_- + \Gamma}{2(1+c_+^2)}\eta^2 + \frac{c_+ + \Gamma}{3(1+c_+^2)}\eta_{xx} - \frac{c_-}{6}\eta_{xx} + \frac{c_-}{2}\theta^2\eta_{xx}. \tag{25}$$

The functions $\xi(t)$ and $\zeta(t)$ are taken to represent the x-coordinate and z-coordinate, respectively, of a particle, initially located at the point $(x,z) = (\xi_0,\zeta_0)$, then the dynamical system is recast in the form

$$\begin{aligned}
&\frac{\partial \xi}{\partial t} = u(\xi(t),\zeta(t),t) - (1+\zeta)\Gamma,\\
&\frac{\partial \zeta}{\partial t} = v(\xi(t),\zeta(t),t),\\
&(\xi(0),\zeta(0)) = (\xi_0,\zeta_0),
\end{aligned} \tag{26}$$

where the effect of an underlying shear-flow has been added. Finally, the particle trajectories are found by numerically integrating the dynamical system (26) using the fourth-order Runge-Kutta method. As explained in [5], for all values of θ, the outcomes will be qualitatively the same in as much as waves are in the validity of the Boussinesq scaling. To get more accurate results in particular cases, Eq. (24) can be used.

3. Particle trajectories in solitary-wave solutions

In this section, we aim to describe the particle trajectories in the fluid owing to the passage of a solitary wave at the surface. The exact solitary-wave solution of the BBM equation (23) is given by

$$\eta(x,t) = \eta_0 \operatorname{sech}^2\left(\sqrt{\frac{3c_+(1+c_+^2)(3+\Gamma^2)\eta_0}{4(c_++\Gamma)[3(1+c_+^2)+(3+\Gamma^2)\eta_0]}}(x-x_0-ct)\right), \tag{27}$$

where η_0 is the initial amplitude, x_0 is the initial location of the wave crest, and the phase velocity is defined as

$$c = c_+ + \frac{c_+(3+\Gamma^2)\eta_0}{3(1+c_+^2)}.$$

In this study, there is an assumption that when $t=0$, the wave crest is located at $x=0$ so that $x_0=0$. Hence, the argument is defined as

$$\mathcal{A}(x,t) = \sqrt{\frac{3c_+(1+c_+^2)(3+\Gamma^2)\eta_0}{4(c_++\Gamma)[3(1+c_+^2)+(3+\Gamma^2)\eta_0]}}(x-ct).$$

Therefore, using Eqs. (25) and (27), the relation (24) gives the horizontal and vertical velocities ($u(x,z,t)$ and $v(x,z,t)$, respectively) of the fluid at $(x, z=-1+\theta(\eta+1))$ in the fluid, at a time t as

$$\begin{aligned}
u = {}& \eta_0\operatorname{sech}^2(\mathcal{A})\left\{-c_- + \frac{3c_+(1+c_+^2)(3+\Gamma^2)\eta_0}{(c_++\Gamma)[3(1+c_+^2)+(3+\Gamma^2)\eta_0]}\left(\frac{c_++\Gamma}{3(1+c_+^2)} - \frac{c_-}{6}\right)\right.\\
&-(1+z)^2\frac{3(1+c_+^2)(3+\Gamma^2)}{(c_++\Gamma)[3(1+c_+^2)+(3+\Gamma^2)\eta_0]}\frac{\eta_0}{2}\\
&+\eta_0\operatorname{sech}^2(\mathcal{A})\left\{\frac{c_-+\Gamma}{2(1+c_+^2)} - \frac{3}{2}\frac{3c_+(1+c_+^2)(3+\Gamma^2)}{(c_++\Gamma)[3(1+c_+^2)+(3+\Gamma^2)\eta_0]}\left(\frac{c_++\Gamma}{3(1+c_+^2)} - \frac{c_-}{6}\right)\right.\\
&\left.\left.+\frac{3}{4}(z+1)^2\frac{3(1+c_+^2)(3+\Gamma^2)}{(c_++\Gamma)[3(1+c_+^2)+(3+\Gamma^2)\eta_0]}\right\}\right.\\
&+\frac{1}{2}\left(\theta^2-(1+z)^2\right)\frac{c_-+\Gamma}{2(1+c_+^2)}\frac{3c_+(1+c_+^2)(3+\Gamma^2)}{(c_++\Gamma)[3(1+c_+^2)+(3+\Gamma^2)\eta_0]}\eta_0^2\operatorname{sech}^2(\mathcal{A})(4-5\operatorname{sech}^2(\mathcal{A}))\\
&-\frac{1}{16}\left(\theta^2-(1+z)^2\right)\frac{9c_+^2(1+c_+^2)^2(3+\Gamma^2)^2\eta_0^2}{(c_++\Gamma)^2[3(1+c_+^2)+(3+\Gamma^2)\eta_0]^2}\times\\
&\left.\left(\frac{c_++\Gamma}{3(1+c_+^2)} - \frac{c_-}{6} + \frac{c_-}{2}\theta^2\right)(-8+60\operatorname{sech}^2\mathcal{A}-60\operatorname{sech}^4\mathcal{A})\right\},\\
v = {}& -(1+z)(\eta_0)^{3/2}\sqrt{\frac{3c_+(1+c_+^2)(3+\Gamma^2)}{4(c_++\Gamma)[3(1+c_+^2)+(3+\Gamma^2)\eta_0]}}\operatorname{sech}^2(\mathcal{A})\tanh(\mathcal{A})\left\{2c_- - \frac{2(c_-+\Gamma)}{(1+c_+^2)}\times\right.\\
&\left.\eta_0\operatorname{sech}^2(\mathcal{A}) + \frac{6c_+(1+c_+^2)(3+\Gamma^2)\eta_0}{(c_++\Gamma)[3(1+c_+^2)+(3+\Gamma^2)\eta_0]}\left(\frac{c_++\Gamma}{3(1+c_+^2)} - \frac{c_-}{6} + \frac{c_-}{2}\theta^2\right)(-1+3\operatorname{sech}^2(\mathcal{A}))\right\}.
\end{aligned} \tag{28}$$

Figs. 2, 3, and 4 show particle trajectories during the propagation of a solitary wave with an amplitude of 0.2 (that is, $\eta_0 = 0.2$). The value of θ used throughout this study is 0.6. The particle paths beneath the solitary waves were obtained

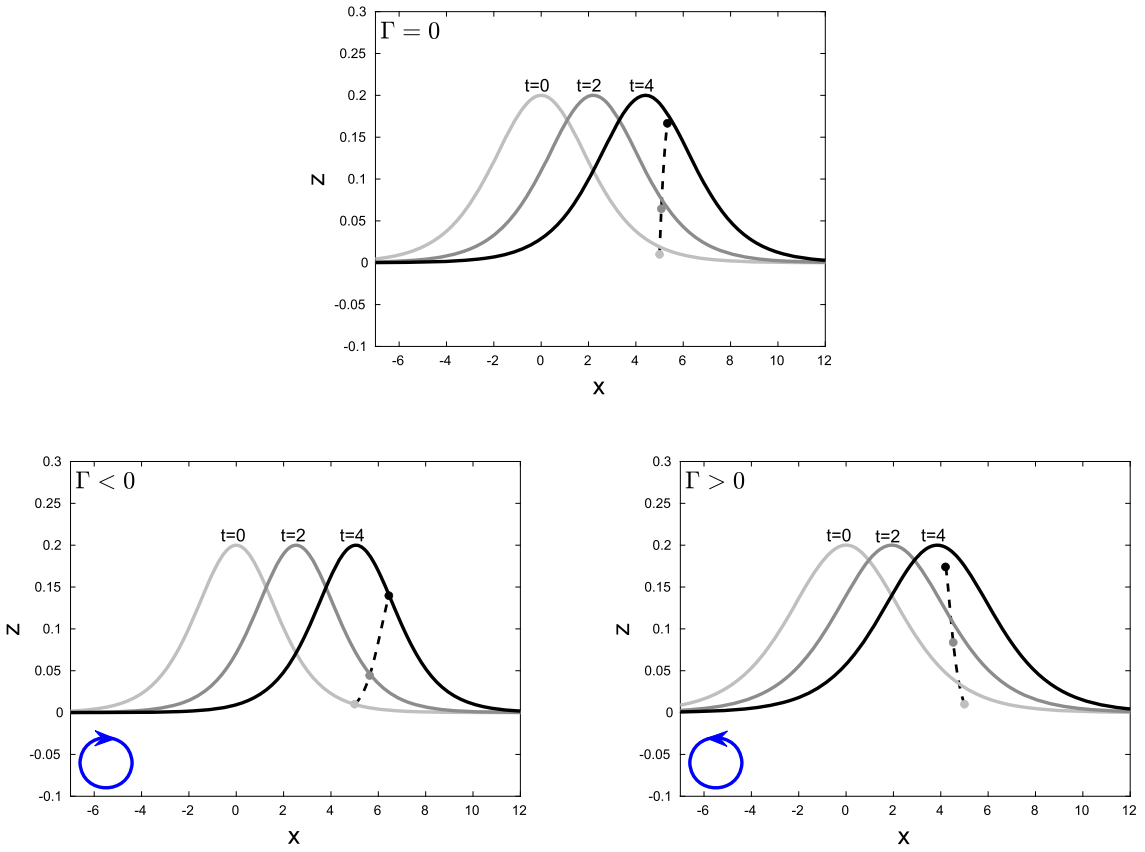

Fig. 2. The waves are shown at time $t = 0$ (light-gray), $t = 2$ (dark-gray), $t = 4$ (black). The wave crest is initially located at $x = 0$. The path of the fluid particles $(\xi(t), \zeta(t))$ of Eq. (26) (u and v corresponds to the Eq. (28)) initially located at (5, 0.01) for different cases of vorticity $\Gamma = 0$; $\Gamma = -0.3$; $\Gamma = 0.3$ are shown. The particle locations at three instances where the wave profile is shown are color coded. The light-gray curve indicates the particle positions at time $t = 0$. The dark-gray curve indicates the particle positions at time $t = 2$. The black curve indicates the particle positions at time $t = 4$. The blue circles indicate the sense of rotation. (For interpretation of the colors in the figure(s), the reader is referred to the web version of this article.)

with the dynamical system (26) where the vector field is given in Eq. (28). In these figures the fluid particle location at the three instances where the wave profile is shown is color-coded: the initial position is indicated by the light-gray dot, the dark-gray dot shows its middle position while the black dot shows its final position. A circle with an arrowhead indicating the sense of rotation of the background shear flow is placed at the bottom of each figure.

Fig. 2 shows the time evolution of a fluid particle located to the right of the crest in the surface for three different vorticity values (a) $\Gamma = 0$; (b) $\Gamma = -0.3$; (c) $\Gamma = 0.3$. The particle path given by equation (26) is represented by the dashed curve. In the case of favorable vorticity ($\Gamma \leq 0$), it can be seen that the fluid particles move to the right and upwards if they are located to the right of the crest, while the fluid particle moves to the left and upwards for the case of vorticity $\Gamma > 0$. This is in agreement with the results of [5,13,24] in the absence of shear flow.

Fig. 3 illustrates particle paths associated to the passage of a solitary wave. It can be seen that the fluid particles closer to the bottom have smaller vertical excursions but nearly the same horizontal extent. Right near the bottom, the particle trajectories become straight lines as the vertical motion becomes zero. The polarity of Γ has a strong influence on the shapes of the particle paths. Indeed, it is apparent from Fig. 3 (lower panels) that the particles in the center of the fluid column move further to the right when $\Gamma < 0$, while particles in the lower half of the fluid column move further to the right when $\Gamma > 0$.

In the upper and left lower panels of Fig. 4, for $\Gamma \leq 0$, fluid particles move to the right and upwards if they are located to the right of the crest and particles located on the left of the crest move to the right and downwards. In the right lower panel of Fig. 4, for $\Gamma > 0$, fluid particles move to the left and upwards if they are located to the right of the crest and particles located on the left of the crest move to the left and downwards. But as can be seen in the right lower panel of Fig. 4, the particles closer to the bottom move to the right and upwards if they are located to the right of the crest and particles located on the left of the crest move to the right and downwards for the case $\Gamma > 0$. It is clear that for particles deeper into the fluid channel, the wave effect diminishes, and therefore the effect due the vorticity can become dominant. Through the numerical simulations, it is apparent that the closer the particle is to the free surface, the stronger it feels the wave effect.

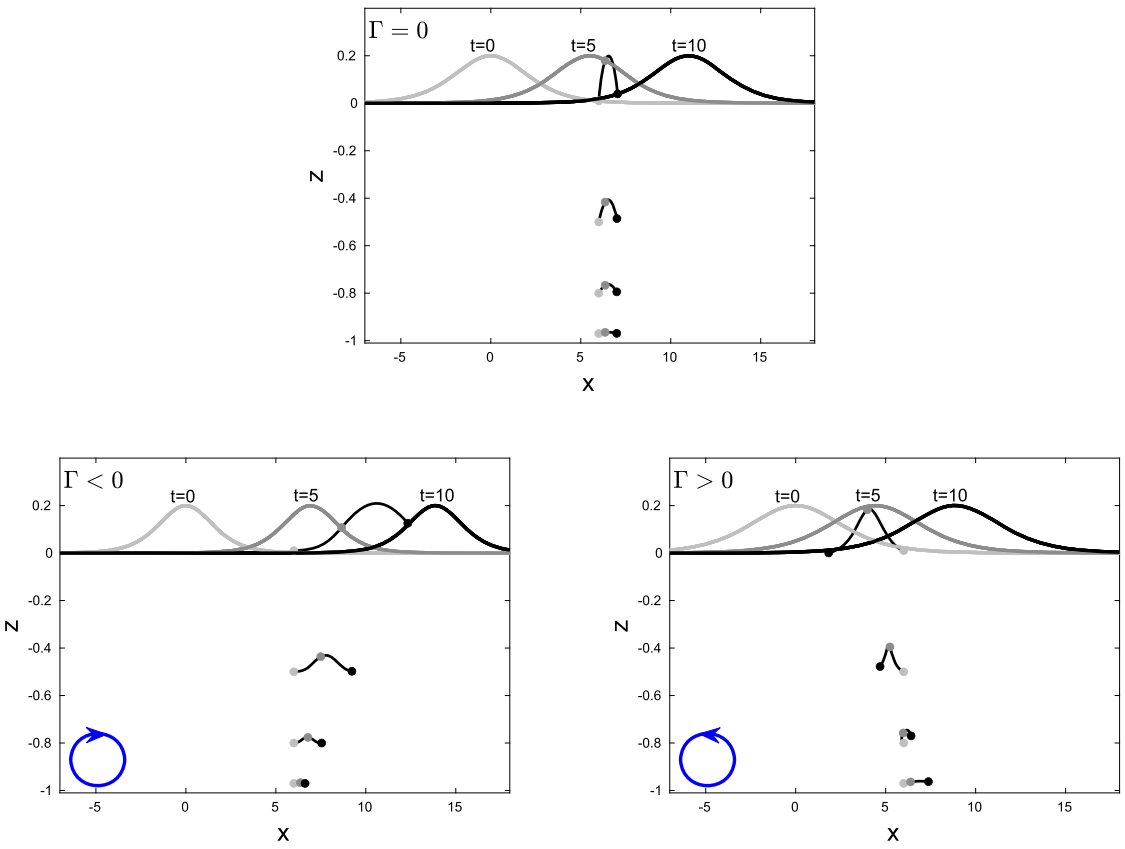

Fig. 3. The waves are shown at time $t = 0$ (light-gray), $t = 5$ (dark-gray), $t = 10$ (black). The wave crest is initially located at $x = 0$. The path of the fluid particles $(\xi(t), \zeta(t))$ in Eq. (26) (u and v corresponds to the Eq. (28)) initially located at (6, -0.97), (6, -0.8), (6, -0.5) and (6, 0.01) are shown for different cases (a) $\Gamma = 0$; (b) $\Gamma = -0.5$; (c) $\Gamma = 0.5$. The particle locations at three instances, where the wave profile is shown, are color-coded. The light-gray dot indicates the particle positions at time $t = 0$. The dark-gray dot indicates the particle positions at time $t = 5$. The black dot indicates the particle positions at time $t = 10$. The blue circles indicate the sense of rotation.

One interesting feature of the present work is that it appears to capture the existence of closed particle orbits in solitary waves such as observed in a field campaign conducted by the Beach Erosion Board on a beach in New Jersey, USA on a gently sloping beach [3]. This finding partially motivated the work of [29], where a solitary wave was coupled with an offshore current in order to capture this phenomenon which is thought to be due to an undertoe. However, an undertoe would more likely be a sheared flow that loses strength in the upper half of the fluid column. If such a flow is introduced in the equation (2), then the resulting flow look like in Fig. 5, where strong beachward transport is seen near the surface, and closed particle orbits exist near the bottom.

4. Particle trajectories in periodic-wave solutions

The focus is now on the particle paths in the fluid flow as a result of the propagation of periodic traveling waves at the surface. The BBM equation (23) admits the following solution in terms of the three constants f_1, f_2, and f_3 which are arranged as $f_3 < f_2 < f_1$, and in terms of cnoidal functions:

$$\eta = f_2 + (f_1 - f_2)\mathrm{cn}^2\left(\sqrt{\frac{3c_+(1+c_+^2)(3+\Gamma^2)}{4(c_++\Gamma)[3(1+c_+^2)+(3+\Gamma^2)(f_1-f_3)]}}(f_1 - f_3)^{1/2}(x - x_0 - ct)\right), \tag{29}$$

where f_1 and f_2 represent the crest and the trough of the wave, respectively. With $x_0 = 0$, the argument is defined as

$$\mathcal{B} = \sqrt{\frac{3c_+(1+c_+^2)(3+\Gamma^2)}{4(c_++\Gamma)[3(1+c_+^2)+(3+\Gamma^2)(f_1-f_3)]}}(f_1 - f_3)^{1/2}(x - ct).$$

Here, cn is one of the Jacobian elliptic functions defined by the incomplete elliptic integral of the first kind [28], where its modulus is defined as $m = (f_1 - f_2)/(f_1 - f_3)$. The phase speed and the wavelength of the wave are given as

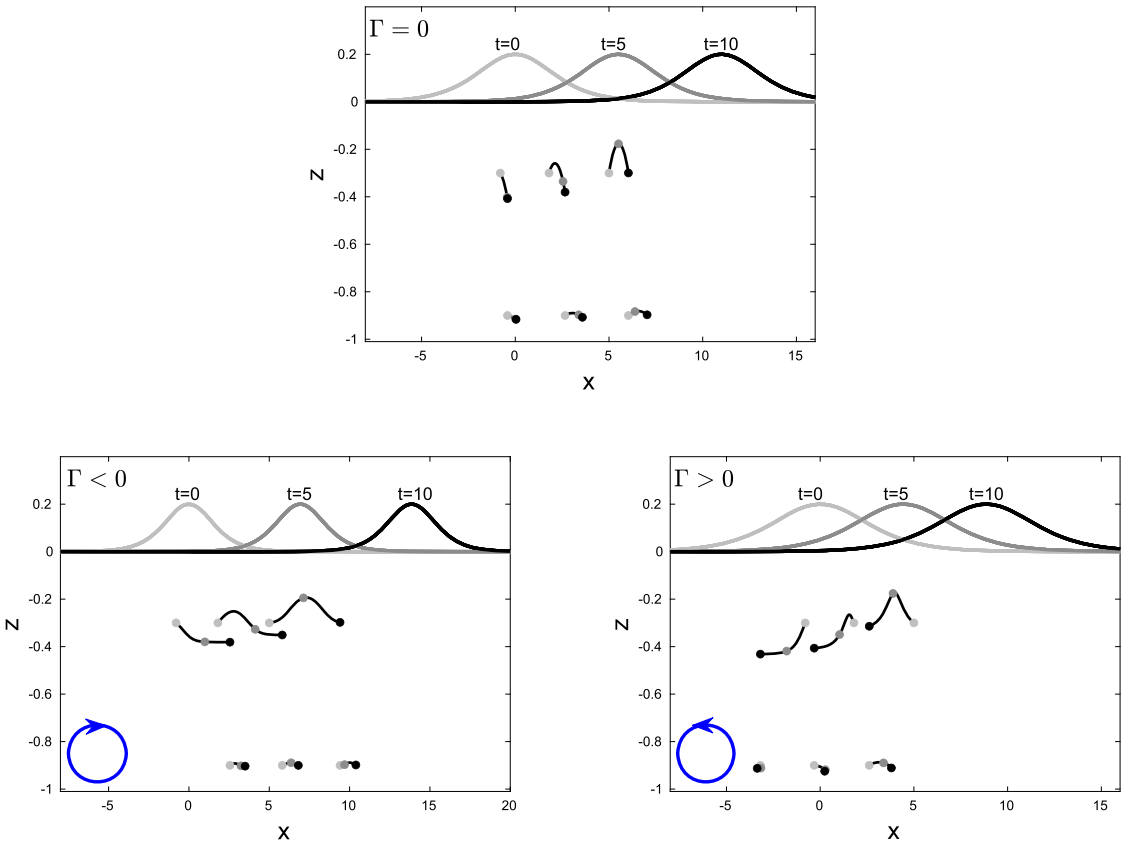

Fig. 4. The waves are shown at time $t = 0$ (light-gray), $t = 5$ (dark-gray), $t = 10$ (black). The wave crest is initially located at $x = 0$. The path of the fluid particles $(\xi(t), \zeta(t))$ in (26) (u and v corresponds to the Eq. (28)) initially located at (-0.8, -0.3), (1.8, -0.3) and (5, -0.3), also (-0.8, -0.9), (1.8, -0.9) and (5, -0.9) are shown for different cases (a) $\Gamma = 0$; (b) $\Gamma = -0.5$; (c) $\Gamma = 0.5$. The particle locations at three instances, where the wave profile is shown, are color-coded. The light-gray curve indicates the particle positions at time $t = 0$. The dark-gray curve indicates the particle positions at time $t = 5$. The black curve indicates the particle positions at time $t = 10$. The blue circles indicate the sense of rotation.

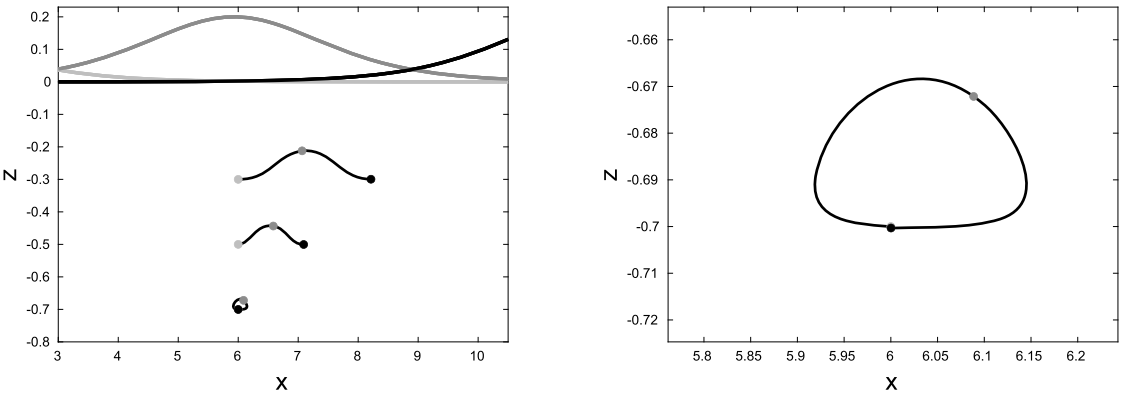

Fig. 5. Solitary-wave solution and particle paths in a shear current. The waves are shown at time $t = 0$ (light-gray), $t = 5$ (dark-gray), $t = 10$ (black). The parameter values are $a = 0.2$, $\Gamma = -0.5$, $U_0 = -0.2$, $c = 1.3859$, $x_0 = 6$. A closed path is visible near the bottom, and a close-up is shown in the right panel.

$$c = c_+ + \frac{c_+(3+\Gamma^2)}{3(1+c_+^2)}(f_1+f_2+f_3),$$

and

$$\lambda = 4\sqrt{\frac{(c_+ + \Gamma)[3(1+c_+^2)+(3+\Gamma^2)(f_1-f_3)]}{3c_+(1+c_+^2)(3+\Gamma^2)}}\,K(m)\frac{1}{\sqrt{f_1-f_3}},$$

respectively, where $K(m)$ is the complete elliptic integral of the first kind. Using Eqs. (25) and (29) in the relations (24), the horizontal and vertical velocities may be written in terms of the Jacobian elliptic functions cn, sn, and dn as

$$
\begin{aligned}
u = &-c_-(f_2+(f_1-f_2)\mathrm{cn}^2(\mathcal{B}))+\frac{c_-+\Gamma}{2(1+c_+^2)}(f_2+(f_1-f_2)\mathrm{cn}^2(\mathcal{B}))^2\\
&+\frac{3c_+(1+c_+^2)(3+\Gamma^2)}{2(c_++\Gamma)[3(1+c_+^2)+(3+\Gamma^2)(f_1-f_3)]}(f_1-f_2)(f_1-f_3)\Big\{\frac{c_++\Gamma}{3(1+c_+^2)}\\
&-\frac{c_-}{6}+\frac{c_-}{2}\theta^2\Big\}\Big\{\mathrm{sn}^2(\mathcal{B})\mathrm{dn}^2(\mathcal{B})-\mathrm{cn}^2(\mathcal{B})\mathrm{dn}^2(\mathcal{B})+m\,\mathrm{sn}^2(\mathcal{B})\mathrm{cn}^2(\mathcal{B})\Big\}\\
&+\Big(\theta^2-(1+z)^2\Big)\frac{3c_+(1+c_+^2)(3+\Gamma^2)}{8(c_++\Gamma)[3(1+c_+^2)+(3+\Gamma^2)(f_1-f_3)]}(f_1-f_3)\\
&\Big\{2c_-(f_1-f_2)\Big(\mathrm{cn}^2(\mathcal{B})\mathrm{dn}^2(\mathcal{B})-\mathrm{sn}^2(\mathcal{B})\mathrm{dn}^2(\mathcal{B})-m\mathrm{sn}^2(\mathcal{B})\mathrm{cn}^2(\mathcal{B})\Big)+2\frac{c_-+\Gamma}{(1+c_+^2)}\times\\
&\quad f_2(f_1-f_2)\Big(\mathrm{sn}^2(\mathcal{B})\mathrm{dn}^2(\mathcal{B})-\mathrm{cn}^2(\mathcal{B})\mathrm{dn}^2(\mathcal{B})+m\mathrm{sn}^2(\mathcal{B})\mathrm{cn}^2(\mathcal{B})\Big)\\
&\quad -2\frac{c_-+\Gamma}{(1+c_+^2)}(f_1-f_2)^2\Big(-m\mathrm{sn}^2(\mathcal{B})\mathrm{cn}^4(\mathcal{B})+\mathrm{cn}^4(\mathcal{B})\mathrm{dn}^2(\mathcal{B})-3\mathrm{sn}^2(\mathcal{B})\mathrm{cn}^2(\mathcal{B})\mathrm{dn}^2(\mathcal{B})\Big)\\
&\quad +\frac{6c_+(1+c_+^2)(3+\Gamma^2)}{(c_++\Gamma)[3(1+c_+^2)+(3+\Gamma^2)(f_1-f_3)]}\left(\frac{c_++\Gamma}{3(1+c_+^2)}-\frac{c_-}{6}+\frac{c_-}{2}\theta^2\right)(f_1-f_2)(f_1-f_3)\times\\
&\quad \Big(-9m\mathrm{sn}^2(\mathcal{B})\mathrm{cn}^2(\mathcal{B})\mathrm{dn}^2(\mathcal{B})-m^2\mathrm{sn}^2(\mathcal{B})\mathrm{cn}^4(\mathcal{B})+m\mathrm{cn}^4(\mathcal{B})\mathrm{dn}^2(\mathcal{B})\\
&\qquad +m^2\mathrm{sn}^4(\mathcal{B})\mathrm{cn}^2(\mathcal{B})+m\mathrm{sn}^4(\mathcal{B})\mathrm{dn}^2(\mathcal{B})+\mathrm{cn}^2(\mathcal{B})\mathrm{dn}^4(\mathcal{B})-\mathrm{sn}^2(\mathcal{B})\mathrm{dn}^4(\mathcal{B})\Big)\Big\},\\
v = &-(1+z)\sqrt{\frac{3c_+(1+c_+^2)(3+\Gamma^2)}{4(c_++\Gamma)[3(1+c_+^2)+(3+\Gamma^2)(f_1-f_3)]}}(f_1-f_3)^{1/2}\mathrm{sn}(\mathcal{B})\mathrm{cn}(\mathcal{B})\mathrm{dn}(\mathcal{B})\{2c_-(f_1-f_2)\\
&-2\frac{c_-+\Gamma}{(1+c_+^2)}f_2(f_1-f_2)-2\frac{c_-+\Gamma}{(1+c_+^2)}(f_1-f_2)^2\mathrm{cn}^2(\mathcal{B})+\left(\frac{c_++\Gamma}{3(1+c_+^2)}-\frac{c_-}{6}+\frac{c_-}{2}\theta^2\right)\times\\
&\frac{6c_+(1+c_+^2)(3+\Gamma^2)}{(c_++\Gamma)[3(1+c_+^2)+(3+\Gamma^2)(f_1-f_3)]}(f_1-f_2)(f_1-f_3)\Big(-m\mathrm{sn}^2(\mathcal{B})+m\mathrm{cn}^2(\mathcal{B})+\mathrm{dn}^2(\mathcal{B})\Big)\Big\}.
\end{aligned}
\tag{30}
$$

The particle paths shown in Figs. 6 - 9 are numerical approximations of solutions of Eq. (26) where the vector field is given in Eq. (30). The cnoidal wave of the BBM equations can be specified by fixing the values of the parameters f_1, f_2, and f_3. Of particular interest is the case of an adverse current, and researchers [14,30] predicted the existence of a closed orbit. Fig. 6 illustrates the particle path during one complete periodic cnoidal wave cycle with $m = 0.99$ and $H = f_1 - f_2 = 0.3$ for different values of vorticity $\Gamma = 0, -0.1$ and 0.1. The crest of the wave is centered at $x = 0$, and depths $z = -0.9, -0.4$ and -0.078. The particle paths are nearly elliptic but not closed in the presence of the vorticity $\Gamma \leq 0$. For the case of positive vorticity $\Gamma > 0$, the particle paths are orbit loops.

Next, we present a train of the cnoidal wave for different values of vorticity $\Gamma = 0, -0.4$, and 0.6. A close-up of particle paths initially located at the surface is shown in Fig. 7. The particle path during the propagation of the cnoidal wave over 4 periods at the three cases are shown, and the initial particle locations are shown in light-gray dots. In the upper and left lower panels of Fig. 7, for $\Gamma \leq 0$, fluid particles move to the right and upwards. As can be seen in the right lower panel of Fig. 7, the particles move to the left and upwards for the case $\Gamma > 0$.

In Figs. 8 and 9, the particle paths with different vorticity values are shown for different depths. In Fig. 8, the particle path during the propagation of the cnoidal wave over one period at the three instances are shown for amplitude 0.2 with different values of vorticity $\Gamma = 0, -0.4$, and 0.6, all particles are initially at $x_0 = \text{wavelength}/2 - 0.001$, and depth $z_0 = -0.1, -0.5$ and -0.9. Fig. 9 features the particle trajectory during the propagation of the cnoidal wave over three periods. The three instances considered are shown for amplitude 0.4 with vorticity $\Gamma = 0, -0.12$, and 0.28. We observe that in the upper and lower panels of Fig. 9, for the particles closer to the bottom, the wave effect diminishes, and therefore the effect due to the vorticity can become dominant.

5. Conclusion

This study has focused on the motion of particles in the body of the fluid excited by the combination of wave motion at the free surface and a pre-existing linear shear flow. The waves were assumed to be long and of small amplitude when

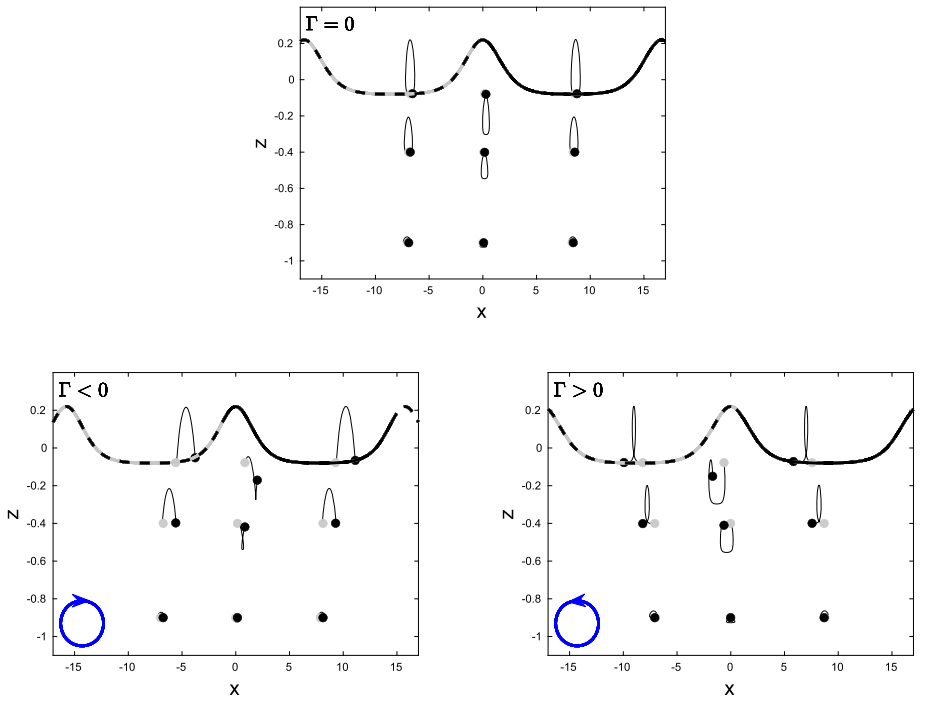

Fig. 6. The upper panel shows the periodic wave with amplitude 0.3, wavelength 16.6372, period 16.1830, phase speed 1.0281 and $\Gamma = 0$ at $t = 0$ (light-gray) and $t = 16.18$ (black). The left lower panel shows the periodic wave with amplitude 0.3, wavelength 15.7511, period 14.5928, phase speed 1.0794 and $\Gamma = -0.1$ at $t = 0$ (light-gray) and $t = 14.59$ (black). The right lower panel shows the periodic wave with amplitude 0.3, wavelength 17.5221, period 17.8910, phase speed 0.9794 and $\Gamma = 0.1$ at $t = 0$ (light-gray) and $t = 17.89$ (black). The paths of fluid particles are located at (x, z), where the initial x-coordinate are $x = -7, 0$ and wavelength$/2 - 0.001$, and depth are $z = -0.9, -0.4$ and -0.078. The blue circles indicate the sense of rotation.

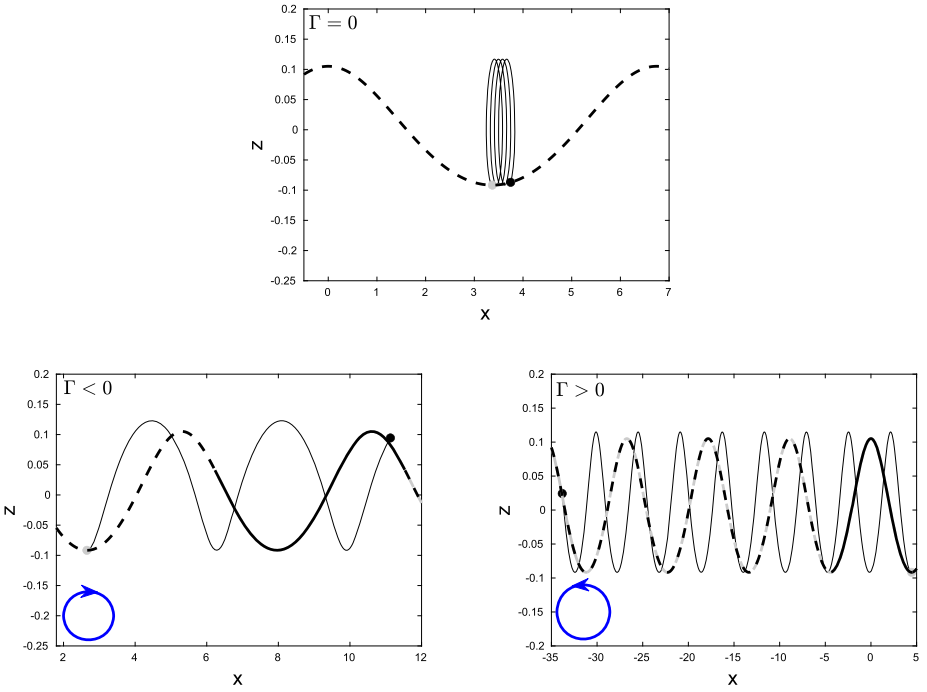

Fig. 7. The upper panel shows the periodic wave with amplitude 0.1968, wavelength 6.7430, period 8.1566, phase speed 0.8267 and $\Gamma = 0$ at $t = 0$ (light-gray) and $t = 4$periods (black), (these values of t are used in all the three cases. This means that the final value of t varies). The left lower panel shows the periodic wave with amplitude 0.1968, wavelength 5.3077, period 5.0997, phase speed 1.0408, and $\Gamma = -0.4$. The right lower panel shows the periodic wave with amplitude 0.1968, wavelength 8.9134, period 15.9709, phase speed 0.5581, and $\Gamma = 0.6$. The initial particle locations at the three cases are shown in light-gray curve. All particles are initially at $x_0 =$ wavelength$/2 - 0.001$ and depth $z_0 = -0.1$. The blue circles indicate the sense of rotation.

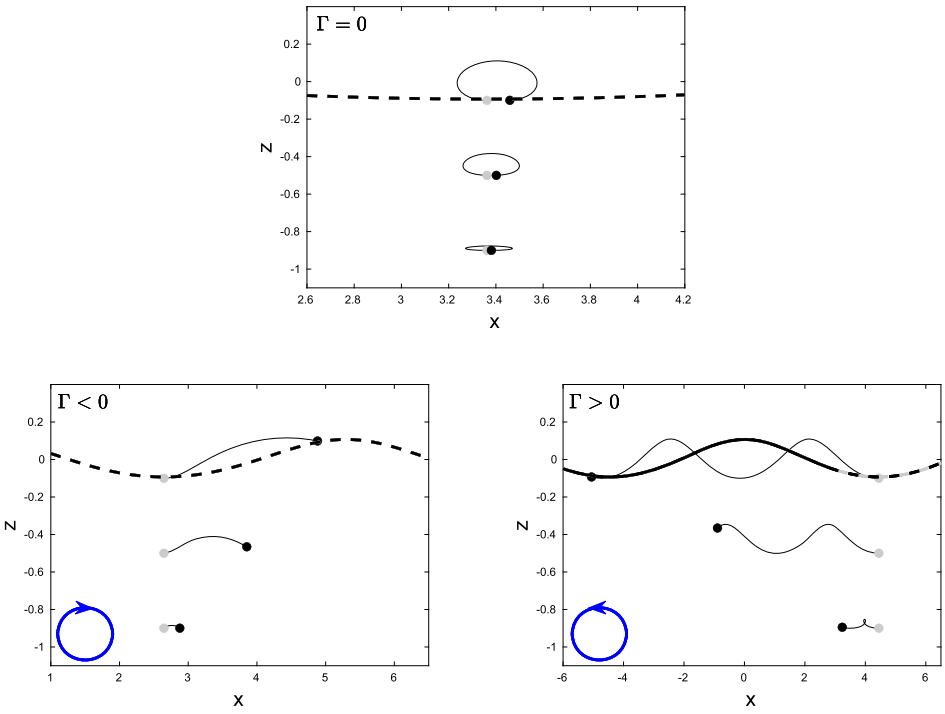

Fig. 8. The upper panel shows the periodic wave with amplitude 0.2, wavelength 6.7264, period 8.1470, phase speed 0.8256, and $\Gamma = 0$ at $t = 0$ (light-gray) and $t = 8.1470$ (black). The left lower panel shows the periodic wave with amplitude 0.2, wavelength 5.2941, period 5.0919, phase speed 1.0397, and $\Gamma = -0.4$ at $t = 0$ (light-gray) and $t = 5.0919$ (black). The right lower panel shows the periodic wave with amplitude 0.2, wavelength 8.8940, period 15.9686, phase speed 0.5570, and $\Gamma = 0.6$ at $t = 0$ (light-gray) and $t = 15.9686$ (black). The initial particle locations in the three cases are shown in the light-gray curve. All particles are initially at $x_0 = \text{wavelength}/2 - 0.001$, and depth $z_0 = -0.1, -0.5$ and -0.9.

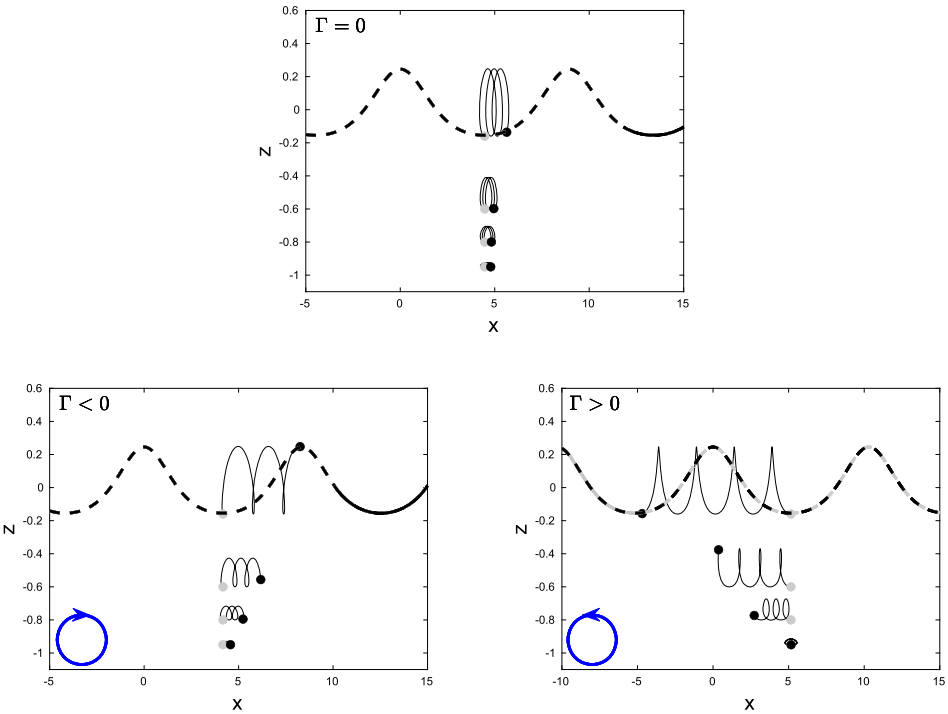

Fig. 9. The upper panel shows the periodic wave with amplitude 0.4 wavelength 8.9389, period 9.5834, phase speed 0.9327, and $\Gamma = 0$ at $t = 0$ (light-gray) and $t = 28.7501$ (black). The left lower panel shows the periodic wave with amplitude 0.4, wavelength 8.3541, period 8.4016, phase speed 0.9943, and $\Gamma = -0.12$ at $t = 0$ (light-gray) and $t = 25.2047$ (black). The right lower panel shows the periodic wave with amplitude 0.4, wavelength 10.3072, period 12.8613, phase speed 0.8014, and $\Gamma = 0.28$ at $t = 0$ (light-gray) and $t = 38.5840$ (black). The initial particle locations are shown in light-gray curve.

compared to the depth of the fluid, so that a weakly nonlinear long-wave equation could be used to describe the wave motion. To this end, a new BBM equation has been derived in the presence of a background shear flow, and expressions for the velocity field of the fluid have been deduced from the derivation. Using the description of the particle paths in terms of a two-by-two system of ordinary differential equations and appropriate discretization techniques, close approximations of particle motions were found for both solitary waves and periodic traveling waves. The influence of the background shear flow on the particle motion was considered, and it was found that the polarity of the associated vorticity has a major effect on the shapes of the trajectories.

We would like to point out that in [21], using a fully nonlinear model, it has been established that the behavior of the particle paths in the presence of background vorticity is associated with the existence of stagnation points in the flow. We have experimented with various parameters, but could not find the existence of internal stagnation points in this weakly nonlinear model equation. However, we were able to find situations with closed particle orbits associated with solitary waves, such as observed in field measurements [29].

References

[1] A. Ali, H. Kalisch, Reconstruction of the pressure in long-wave models with constant vorticity, Eur. J. Mech. B, Fluids 37 (2013) 187–194.
[2] M. Bakhoday-Paskyabi, Particle motions beneath irrotational water waves, Ocean Dyn. 65 (8) (2015) 1063–1078.
[3] Beach Erosion Board, A summary of the theory of oscillatory waves, Technical Report No. 2, United States Government Printing Office, 1942.
[4] T.B. Benjamin, The solitary wave on a stream with an arbitrary distribution of vorticity, J. Fluid Mech. 12 (1962) 97–116.
[5] H. Borluk, H. Kalisch, Particle dynamics in the KdV approximation, Wave Motion 49 (2012) 691–709.
[6] M. Bjørnestad, M. Buckley, H. Kalisch, M. Streßer, J. Horstmann, H.G. Frøysa, O.E. Ige, M. Cysewski, R. Carrasco-Alvarez, Lagrangian measurements of orbital velocities in the surf zone, Geophys. Res. Lett. 48 (2021) e2021GL095722.
[7] J.C. Burns, Long waves in running water, Math. Proc. Camb. Philos. Soc. 49 (4) (1953) 695–706.
[8] A. Castro, D. Lannes, Well-posedness and shallow-water stability for a new Hamiltonian formulation of the water waves equations with vorticity, Indiana Univ. Math. J. 64 (2015) 1169–1270.
[9] L. Chen, B. Basu, C.I. Martin, On rotational flows with discontinuous vorticity beneath steady water waves near stagnation, J. Fluid Mech. 912 (2021) A44.
[10] Y.-Y. Chen, H.-C. Hsu, G.-Y. Chen, Lagrangian experiment and solution for irrotational finite-amplitude progressive gravity waves at uniform depth, Fluid Dyn. Res. 42 (2010) 045511.
[11] W. Choi, Strongly nonlinear long gravity waves in uniform shear flows, Phys. Rev. E 68 (2003).
[12] A. Constantin, The trajectories of particles in Stokes waves, Invent. Math. 166 (3) (2006) 523–535.
[13] A. Constantin, J. Escher, Particle trajectories in solitary water waves, Bull. Am. Math. Soc. 44 (2007) 423–431.
[14] A. Constantin, W. Strauss, Pressure beneath a Stokes wave, Commun. Pure Appl. Math. 63 (4) (2010) 533–557.
[15] A. Constantin, G.J. Villari, Particle trajectories in linear water waves, J. Math. Fluid Mech. 10 (2008) 1–18.
[16] D. Crowdy, Explicit solutions for a steady vortex-wave interaction, J. Fluid Mech. 513 (2004) 161–170.
[17] C.W. Curtis, J.D. Carter, H. Kalisch, Particle paths in nonlinear Schrödinger models in the presence of linear shear currents, J. Fluid Mech. 855 (2018) 322–350.
[18] C.W. Curtis, H. Kalisch, Vortex dynamics in nonlinear free surface flows, Phys. Fluids 29 (2017) 032101.
[19] L. Debnath, Nonlinear Water Waves, Academic Press Inc., 1994.
[20] F.J. Gerstner, Theory of Waves, Abhandlungen der Königl, Böhmischen Gesellschaft der Wissenschaften zu Prag, 1802.
[21] X. Guan, Particle trajectories under interactions between solitary waves and a linear shear current, Theor. Appl. Mech. Lett. 10 (2) (2020) 125–131.
[22] D. Henry, On Gerstner's water wave, J. Nonlinear Math. Phys. 15 (2) (2008) 87–95.
[23] H.C. Hsu, Particle trajectories for waves on a linear shear current, Nonlinear Anal., Real World Appl. 14 (2013).
[24] O.E. Ige, Z. Khorsand, Particle trajectories in the BBM approximation, IAENG Int. J. Appl. Math. 50 (3) (2020) 589–600.
[25] C. Kharif, M. Abid, Nonlinear water waves in shallow water in the presence of constant vorticity: a Whitham approach, Eur. J. Mech. B, Fluids 72 (2018) 12–22.
[26] L.F. Kilcher, J.D. Nash, Structure and dynamics of the Columbia river tidal plume front, J. Geophys. Res., Oceans 115 (2010) C05590.
[27] H. Lamb, Hydrodynamics, Dover Publications, New York, 1945.
[28] D.F. Lawden, Elliptic Functions and Applications, Springer, New York, 1989.
[29] W.H. Munk, The solitary wave theory and its application to surf problems, Ann. N.Y. Acad. Sci. 51 (1949) 376–424.
[30] A. Nachbin, R. Ribeiro-Junior, A boundary integral formulation for particle trajectories in Stokes waves, Discrete Contin. Dyn. Syst. 34 (8) (2014) 3135–3153.
[31] R. Ribeiro, P.A. Milewski, A. Nachbin, Flow structure beneath rotational water waves with stagnation points, J. Fluid Mech. 812 (2017) 792–814.
[32] A. Senthilkumar, H. Kalisch, Wave breaking in the KdV equation on a flow with constant vorticity, Eur. J. Mech. B, Fluids 73 (2019) 48–54.
[33] J.J. Stoker, Water Waves. The Mathematical Theory with Applications, Interscience Publ. Inc., New York, 1957.
[34] G.G. Stokes, On the Theory of Oscillatory Waves, Trans. Camb. Phil. Soc., 1847, pp. 441–455. Reprinted in: G.G. Stokes, Mathematical and Physical Papers, vol. I, Cambridge University Press, 1880, pp. 197–229.
[35] J. Shatah, S. Walsh, C. Zeng, Travelling water waves with compactly supported vorticity, Nonlinearity 26 (2013) 1529.
[36] R. Stuhlmeier, Effects of shear flow on KdV balance - applications to tsunami, Commun. Pure Appl. Anal. 11 (2012) 1549–1561.
[37] A.F. Teles da Silva, D.H. Peregrine, Steep, steady surface waves on water of finite depth with constant vorticity, J. Fluid Mech. 195 (1988) 281–302.
[38] R. Thomas, C. Kharif, M. Manna, A nonlinear Schroedinger equation for water waves on finite depth with constant vorticity, Phys. Fluids 24 (2012) 127102.
[39] F. Ursell, Mass transport in gravity waves, Proc. Camb. Philol. Soc. 40 (1953) 145–150.
[40] V. Vasan, K. Oliveras, Pressure beneath a traveling wave with constant vorticity, Discrete Contin. Dyn. Syst. 34 (2014) 3219–3239.
[41] Z. Wang, X. Guan, J.M. Vanden-Broeck, Progressive flexural-gravity waves with constant vorticity, J. Fluid Mech. 905 (2020).
[42] C. Yaosong, L. Guocan, J. Tao, Non-linear water waves on shearing flows, Acta Mech. Sin. 10 (2) (1994) 97–102.